

Structure and superconductivity of two different phases of Re_3W

P.K. Biswas,^{1,*} M.R. Lees,¹ A.D. Hillier,² R.I. Smith,² W.G. Marshall,² and D.McK. Paul¹

¹*Physics Department, University of Warwick, Coventry, CV4 7AL, United Kingdom*

²*ISIS Facility, Science and Technology Facilities Council,*

Rutherford Appleton Laboratory, Chilton, Oxfordshire, OX11 0QX, U.K.

(Dated: November 6, 2018)

Two superconducting phases of Re_3W have been found with different physical properties. One phase crystallizes in a non-centrosymmetric cubic (α -Mn) structure and has a superconducting transition temperature, T_c , of 7.8 K. The other phase has a hexagonal centrosymmetric structure and is superconducting with a T_c of 9.4 K. Switching between the two phases is possible by annealing the sample or remelting it. The properties of both phases of Re_3W have been characterized by powder neutron diffraction, magnetization, and resistivity measurements. The temperature dependence of the lower and the upper critical fields have been measured for both phases. These are used to determine the penetration depths and the coherence lengths for these systems.

PACS numbers: 74.25.Ha, 74.25.fc, 74.25.Op, 74.70.Ad

I. INTRODUCTION

The discovery of superconductivity in the non-centrosymmetric (NCS) heavy fermion CePt_3Si (Ref. 1) has resulted in a period of intense theoretical and experimental investigation into the physics of non-centrosymmetric superconducting materials. The lack of inversion symmetry in the crystal structure of this type of material along with strong spin-orbit (SO) coupling can lead to a mixing of spin-singlet and spin-triplet pair states². These NCS materials exhibit unusual magnetic properties including suppressed paramagnetic limiting or high upper critical fields^{3,4} as seen in CePt_3Si ,¹ CeRhSi_3 ,⁵ and CeIrSi_3 ,⁶ the appearance of superconductivity with antiferromagnet order in CePt_3Si ,⁷ and superconductivity at the border of ferromagnetism in UIr .⁸

One recent focus of the work on non-centrosymmetric superconductors has been to investigate the properties of transition-metal compounds that have a significant spin-orbit coupling. Here, the complications of the f -electron heavy fermions, such as the strong electron correlations and the possibility of magnetically mediated superconductivity, are expected to be absent. The intermetallic Re_3W belongs in this category since it contains heavy atoms with atomic numbers 75 and 74 for Re and W respectively. Superconductivity in Re_3W was first reported in the 1960's. The material was shown to have a cubic α -Mn structure,^{9,10} although it is worth noting that the authors of this early work did not comment on the fact that the α -Mn structure is non-centrosymmetric. Since then, very little experimental work has been done on Re_3W . Recent penetration depth measurements carried out on the NCS phase of Re_3W by rf tunnel diode resonator and point-contact spectroscopy suggested that Re_3W is a weakly coupled isotropic s-wave superconductor.¹¹⁻¹³

In this paper, we report on the synthesis of two different superconducting phases of Re_3W . One phase has a centrosymmetric (CS) crystal structure, whereas the other has a non-centrosymmetric structure. Switching

from the CS to the NCS phase is achieved by annealing the sample, while remelting the NCS sample in an arc furnace returns the sample to the CS structure. The ease with which one can switch between the two phases of Re_3W has allowed us to investigate and compare the properties of a CS and a NCS superconducting system using a single material without changes in stoichiometry. We characterize the properties of both phases of Re_3W using neutron diffraction, magnetization, M , and resistivity, ρ , measurements. We present the temperature dependence of the lower critical field, H_{c1} , and the upper critical field, H_{c2} , of both materials and also calculate the penetration depths and coherence lengths for these systems.

II. SAMPLE PREPARATION

Samples of the centrosymmetric phase of Re_3W were prepared by melting together a stoichiometric mixture of Re lumps (99.99%) and W pieces (99.999%) in an arc furnace on a water-cooled copper hearth using tungsten electrodes in a high-purity Ar atmosphere. After the initial melt, the buttons were turned and remelted several times to ensure homogeneity. Samples of the non-centrosymmetric phase were made by annealing the as-grown samples for 5 days at 1500°C in a high-purity Ar atmosphere. The unannealed samples of Re_3W are hard but malleable. The samples become brittle after annealing.

III. RESULTS AND DISCUSSION

A. Powder neutron diffraction studies

Time-of-flight powder neutron diffraction data were collected on the General Materials Diffractometer (GEM) at the ISIS Facility in the Rutherford Appleton Laboratory. UK¹⁴ The data were normalized to the inci-

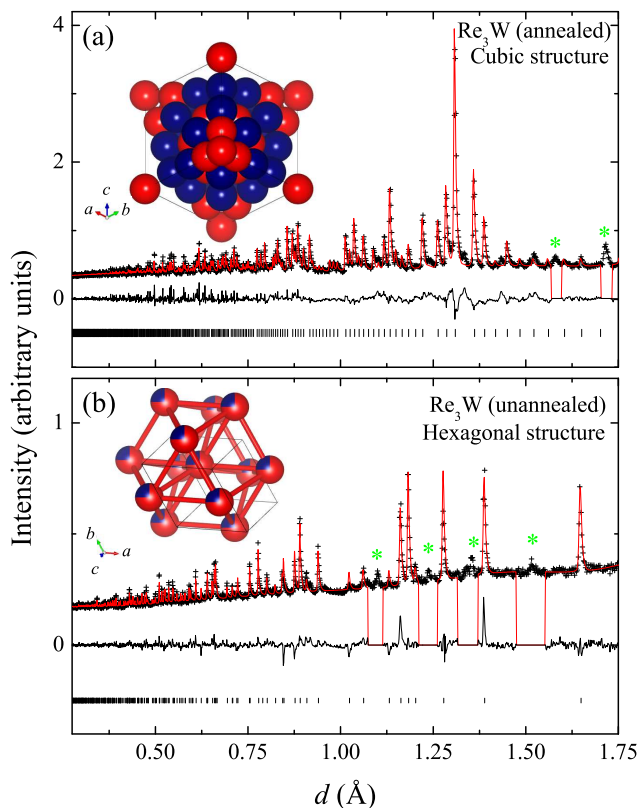


FIG. 1: (Color online) Neutron diffraction patterns as a function of d -spacing collected at 295 K for the annealed and unannealed samples of Re_3W . The experimental data (crosses) are shown along with the calculated pattern obtained from a Rietveld refinement of the structure and a difference curve. The ticks indicate positions of the nuclear Bragg peaks. The green asterisks mark the positions of impurity peaks. The Rietveld refinement shows that the annealed sample has a non-centrosymmetric cubic structure while the unannealed sample has a centrosymmetric hexagonal structure. Insets show the crystal structures of the two phases, with the Re atoms shown in red (light gray) and the W atoms shown in blue (dark gray).

dent neutron flux distribution and corrected for detector efficiencies and detector solid angle coverage, with the diffraction patterns collected in the highest resolution backscattering detector bank (average $2\theta = 154^\circ$) used for structure refinement. Crystal structures were refined by the Rietveld method using the EXPGUI graphical interface for the GSAS package^{15,16}. Figure 1 shows the diffraction patterns collected at 295 K from the annealed and unannealed samples of Re_3W . The Rietveld refinement shows that the annealed sample has a cubic NCS (α -Mn) structure (space group $I\bar{4}3m$) with a lattice parameter $a = 9.5987(7)$ Å [see Fig. 1(a)]. The diffraction pattern of the unannealed sample shows that this sample has a hexagonal structure with the CS space group $P6_3/mmc$ and lattice parameters $a = 2.770(3)$ Å and $c = 4.5207(6)$ Å [see Fig. 1(b)]. The diffraction patterns of both phases of Re_3W contain some peaks (denoted by

TABLE I: Lattice parameters of the non-centrosymmetric and centrosymmetric phases of Re_3W determined from a structural refinement using the GSAS package of powder neutron diffraction data collected at 295 K.

	NCS Re_3W	CS Re_3W
Structure	Cubic	Hexagonal
Space group	$I\bar{4}3m$	$P6_3/mmc$
a (Å)	9.5987(7)	2.770(3)
c (Å)		4.5207(6)
V_{cell} (Å ³)	884.37(2)	30.04(5)
R_p	0.049	0.077
wR_p	0.0697	0.1

TABLE II: Atomic position parameters of the non-centrosymmetric and centrosymmetric phases of Re_3W determined from a structural refinement using the GSAS package of powder neutron diffraction data collected at 295 K

NCS Re_3W						
Atom	Site	x	y	z	Occ.	U_{iso} (Å ²)
Re	2a	0	0	0	0.99(4)	0.070(5)
W	8c	0.3192(3)	0.3192(3)	0.3192(3)	1.00	0.0068(7)
W	24g	0.3605(1)	0.3605(1)	0.0455(1)	0.21(2)	0.0090(3)
Re	24g	0.3605(1)	0.3605(1)	0.0455(1)	0.78(1)	0.0090(3)
Re	24g	0.0910(1)	0.0910(1)	0.2825(1)	1.00	0.0089(2)
CS Re_3W						
Atom		x	y	z	Occ.	U_{iso} (Å ²)
Re	2c	0.3333	0.6667	0.25	0.75	0.0025(1)
W	2c	0.3333	0.6667	0.25	0.25	0.0025(1)

asterisks) that cannot be indexed, and these regions were excluded during the final stages of structure refinement. Insets of Figs. 1(a) and 1(b) show the crystal structures of the NCS and the CS phases of Re_3W . For the CS phase of Re_3W , both the Re and the W atoms share the same site leading to a random distribution of Re and W within the material. For the NCS phase, the refinement indicates that Re and the W atoms occupy preferred crystallographic sites and are therefore distributed in a more orderly fashion within the material. The refined composition of the NCS phase is not stoichiometric indicating there is still some uncertainty in the site occupation. Crystallographic parameters of the two phases of Re_3W are shown in Tables I and II.

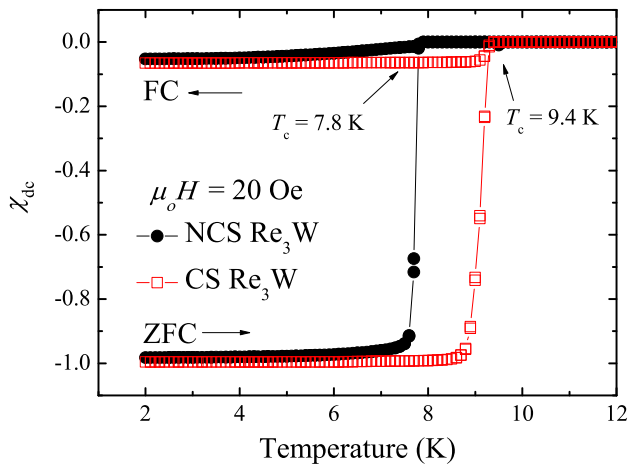


FIG. 2: (Color online) Temperature dependence of the magnetic susceptibility for the non-centrosymmetric and the centrosymmetric Re_3W measured in zero-field-cooled and field-cooled mode in an applied magnetic field of 20 Oe.

B. Magnetization and resistivity measurements

Magnetization measurements were made as a function of temperature in an applied magnetic field of 20 Oe using a Quantum Design Magnetic Property Measurement System (MPMS) magnetometer. The temperature dependence of the dc magnetic susceptibility, $\chi_{\text{dc}}(T)$, shows that the NCS Re_3W sample has a superconducting transition temperature, T_c^{onset} , of 7.8 K [see Fig. 2] with a transition width $\Delta T_c = 0.21$ K. For CS Re_3W , the onset of the transition is around 9.4 K with a much broader transition of $\Delta T_c = 0.50$ K. Comparable transition widths are observed in the resistivity measurements (see below). This suggests, as expected, that the annealed NCS phase of Re_3W is more ordered than the unannealed CS phase. At 2 K, the zero-field-cooled (ZFC) dc susceptibility approaches a value of -1 ($\sim 100\%$ shielding effect) for both the samples, while the field-cooled (FC) signal shows a flux exclusion (Meissner effect) of $\sim 5\%$ for the NCS phase and $\sim 7\%$ for the CS phase.

The ac electrical resistivity was measured as a function of temperature, $\rho(T)$, for both phases of Re_3W via a standard four-probe method using a Quantum Design Physical Property Measurement System (PPMS) [see Fig. 3]. The NCS Re_3W shows a superconducting transition (onset) at 7.85 K ($\Delta T_c = 0.05$ K) while the CS Re_3W has a transition at 9.45 K ($\Delta T_c = 0.32$ K). The zero-field onset transition temperatures determined from the resistivity measurements are slightly higher than those obtained from the magnetization measurements performed in 20 Oe. The resistivity curves between 2 and 295 K show metallic behavior for the CS phase of Re_3W , whereas it is almost temperature independent above T_c in the NCS phase of Re_3W [see the inset of Fig. 3]. The relative

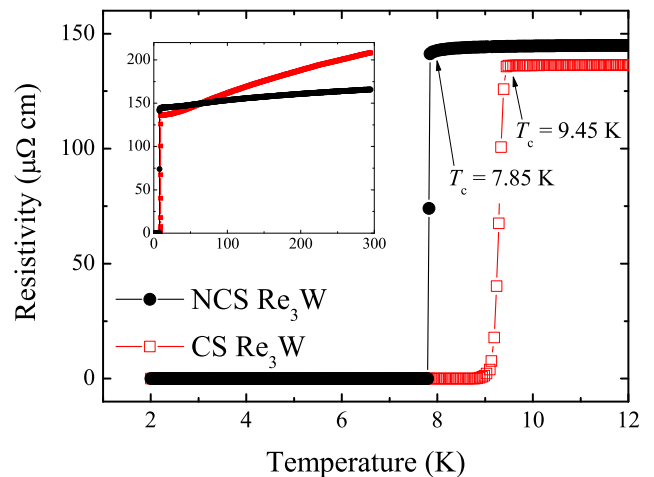


FIG. 3: (Color online) Low-temperature ac electrical resistivity of the NCS and the CS phases of Re_3W . The inset shows the electrical resistivity of both phases up to room temperature.

resistance ratio, $\rho(295 \text{ K})/\rho(10 \text{ K})$ and the room temperature resistivity are 1.15(1) and $1.7\mu\Omega\text{m}$ for the NCS phase and 1.52(1) and $2.1\mu\Omega\text{m}$ for the CS phase, indicating that both samples are poor metals. The NCS phase is the more brittle of the two materials and any extrinsic factors such as microscopic cracks in the sample are more likely to play a role in this material. Given that the room temperature resistivity of the NCS sample is lower than the CS phase we suggest that cracks are not the reason for the high normal-state resistivity. The poor conductivity is more likely to result from a combination of strong electronic scattering and a large temperature independent residual resistivity due to structural disorder (while the NCS annealed phase is structurally more ordered than the CS phase, the NCS phase still retains a degree of Re/W disorder). We have calculated the mean free path, l_{tr} , based on the BCS approach¹⁷ using the room temperature resistivity data. The calculations yield $l_{tr}^{\text{NCS}} = 0.277$ nm and $l_{tr}^{\text{CS}} = 0.224$ nm. These values are comparable with size of the crystallographic unit cells and given the coherence lengths, ξ , derived below, indicate that both phases of Re_3W are in the dirty limit.

Figs. 4(a) and (b) show the low-field virgin magnetization data for the NCS and CS phases of Re_3W at 1.8 K and figures 5(a) and (b) show the full magnetization versus applied magnetic field loops collected in the superconducting state at 1.8 K. For the NCS sample the raw $M(H)$ data contain a significant paramagnetic contribution. This contribution has been removed from the data shown in Fig. 5(a) by measuring an $M(H)$ curve above T_c at 10 K (see inset of Fig. 5(a)). The signal for the CS sample contains a small linear susceptibility $\chi_{\text{dc}} = 3.53 \times 10^{-3}$ emu/mol (see inset of Fig. 5(b)) that has been subtracted from the data shown in figure 5(b). For the NCS sample, the value of H_p (complete pene-

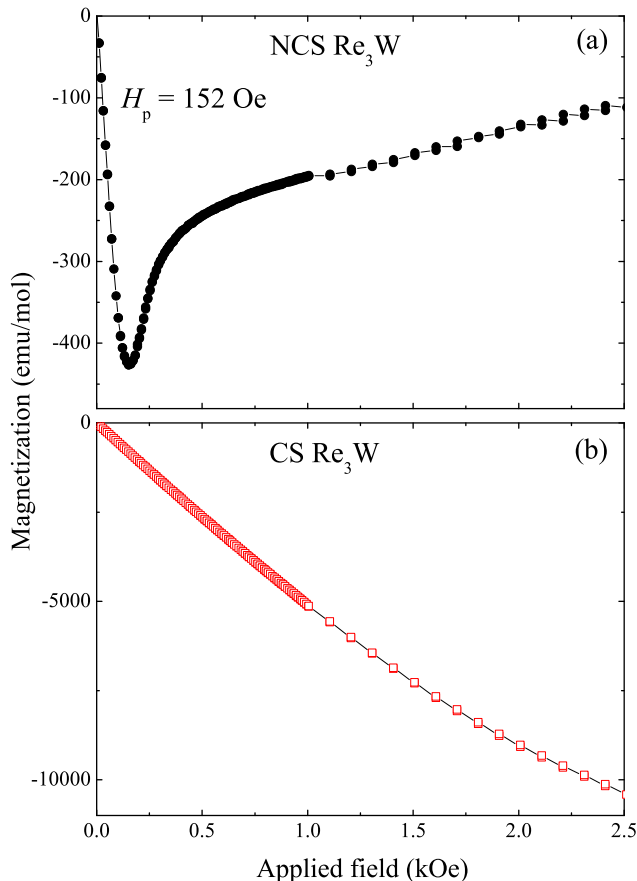


FIG. 4: (Color online) Virgin magnetization curves measured at 1.8 K for the (a) non-centrosymmetric and (b) centrosymmetric phases of Re_3W .

tration of the magnetic field) is 152 Oe while in the CS sample, $H_p > 2500$ Oe. For the NCS phase of Re_3W the magnetization is reversible all the way from 70 kOe, the highest field that we can apply in our magnetometer, down to 10 kOe. We presume that the magnetization will remain reversible up to the upper critical field, estimated from the resistance measurements presented below to be 113 kOe at $T = 1.8$ K. In contrast, the magnetization of the CS sample only becomes reversible in magnetic fields above 40 kOe (with $H_{c2}(T = 1.8 \text{ K}) \approx 130$ kOe). For lower fields the hysteresis loops of the CS sample contain a number of large magnetic-flux jumps, while no jumps are observed for the annealed samples. These flux jumps occur at lower temperatures ($T \leq 4$ K) and at applied fields below ~ 20 kOe. The number and magnitude of the flux jumps vary from loop to loop and become less frequent as the field sweeping rate, dH/dt , is decreased (data not shown). At 5 K with ($dH/dt \leq 10$ Oe/s) no flux jumps are observed and at higher temperatures ($5 \text{ K} < T < T_c$) the flux jumps disappear.

The $M(H)$ curves show that both Re_3W phases exhibit reversible behavior below T_c over a large region of

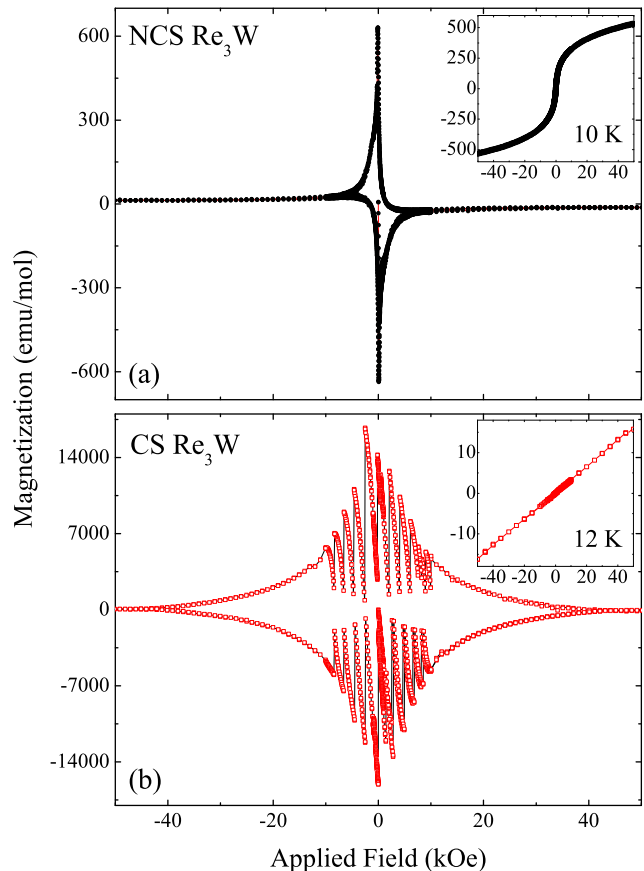


FIG. 5: (Color online) Magnetization hysteresis loops at 1.8 K for the (a) NCS and (b) CS phases of Re_3W . The insets show the $M(H)$ curves for the samples above T_c .

the H - T phase diagram. These data indicate that the bulk pinning is stronger in the CS phase of Re_3W than the NCS phase, and that the flux jumps are due to thermomagnetic instabilities induced by the motion of vortices into the superconductor combined with the sudden redistribution of the vortices within the sample¹⁸. The symmetry of the loops suggests that surface barriers do not play an important role in determining the form of the magnetization loops in this material. Further studies are underway to investigate the different pinning mechanisms in the two different phases of Re_3W .

The value of the lower critical field, H_{c1} , was determined by measuring the field of first deviation from the initial slope of the magnetization curve. To this end, a linear fit to the data between 0 and 10 Oe was made. The deviation from linearity, ΔM , was then calculated by subtracting this fit from the magnetization curves and plotted as a function of applied field [see Figs. 6(a) and 6(b)]. The temperature dependence of H_{c1} for the two phases of Re_3W are obtained by using the criterion $\Delta M = 10^{-4}$ emu/mol and plotted in Figs. 6(c) and 6(d). Demagnetizing effects are taken into ac-

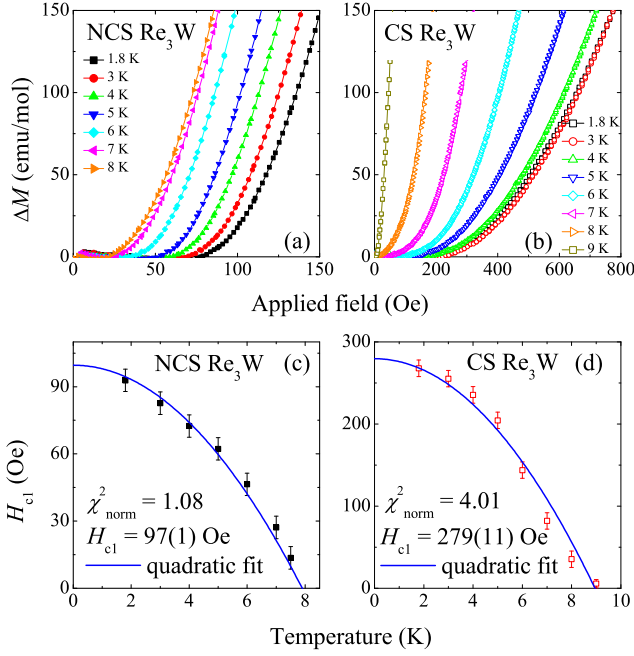


FIG. 6: (Color online) Deviation, ΔM , from the linear virgin magnetization as a function of applied field determined at different temperatures for the (a) NCS and (b) CS phases of Re_3W . H_{c1} as a function of temperature for the (c) NCS and (d) CS phases of Re_3W . The solid lines are fits to the data using the expression $H_{c1}(T) = H_{c1}(0) \{1 - (T/T_c)^2\}$.

count in estimating the H_{c1} values. The values determined for both the samples are fitted using the expression $H_{c1}(T) = H_{c1}(0) \{1 - (T/T_c)^2\}$, where $H_{c1}(0)$ is the lower critical field at zero temperature. The quadratic equation fits the data well for the NCS phase, whereas the model provides a poor fit to the data of the CS phase. The fits yield $H_{c1}(0)$ of 97(1) and 279(11) Oe for the NCS and the CS samples respectively.

Resistivity measurements as a function of temperature were made in magnetic fields up to 90 kOe on both the NCS and the CS samples of Re_3W [see Fig. 7 (a) and (b)]. In the normal state just above T_c , both phases exhibit a small ($\sim 0.6\%$) positive magnetoresistance in a magnetic field of 90 kOe. The temperature dependence of the upper critical field, $H_{c2}(T)$, of the NCS and the CS samples, determined from the onset of the resistive transitions (defined by a 1% drop of the resistivity), are shown in Fig. 7 (c) and (d). For the NCS sample, the temperature dependence of H_{c2} is nearly linear close to T_c with $dH_{c2}^{\text{NCS}}/dT = -23.0(2)$ kOe/K and can be described using the Werthamer-Helfand-Hohenberg (WHH) model^{19,20}. In fitting the data to the WHH relations we calculated the Maki parameter, $\alpha = 1.41$, compared with a value of 1.22 estimated from the gradient dH_{c2}^{NCS}/dT near T_c . The WHH fit yields $H_{c2}^{\text{NCS}} = 125(1)$ kOe at $T = 0$ K. The temperature dependence of H_{c2} for the CS sample clearly shows a difference in behav-

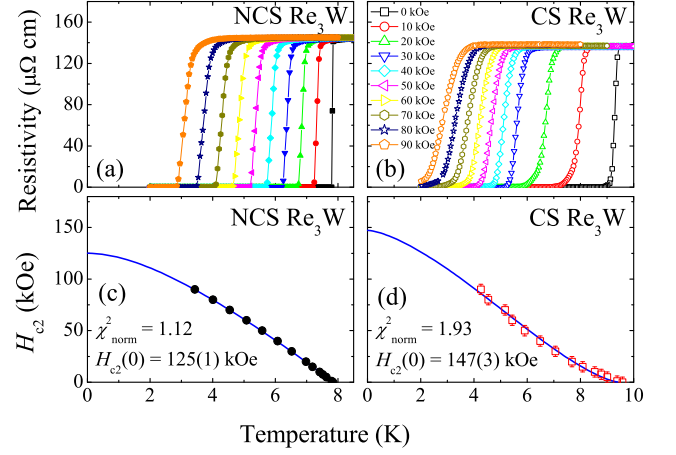


FIG. 7: (Color online) Temperature variation of the resistivity in a set of magnetic fields from 0 to 90 kOe for the (a) NCS and (b) CS phases of Re_3W . Temperature dependence of the upper critical fields of the (c) NCS and (d) CS phases of Re_3W . The solid line in (c) is a fit to the data using the WHH model. The solid line in (d) is a fit to the data using $H_{c2}(T) = H_{c2}(0)(1 - (T/T_c)^{3/2})^{3/2}$.

ior compared to the NCS sample with deviations from the conventional WHH dependence. The data have a positive curvature with temperature near T_c and are linear thereafter. A similar behavior is observed in polycrystalline borocarbides²¹, MgB_2 ^{22,23}, and $\text{Nb}_{0.18}\text{Re}_{0.82}$.²⁴ A reasonable fit to the data for the CS sample can be obtained using the expression $H_{c2}(T) = H_{c2}(0)(1 - (T/T_c)^{3/2})^{3/2}$ giving $H_{c2}^{\text{CS}}(0) = 147(3)$ kOe²⁵. A simple linear extrapolation of the lower temperature data to $T = 0$ K gives $H_{c2}^{\text{CS}}(0) = 178(5)$ kOe with $dH_{c2}^{\text{CS}}/dT = -21(1)$ kOe/K. A similar analysis of the data for the NCS sample gives $H_{c2}^{\text{NCS}}(0) = 153(1)$ kOe. While the temperature dependence of H_{c2} for the two phases is clearly different, the values of H_{c2} at $T = 0$ K are comparable. The analysis presented above shows that $H_{c2}(0)$ appears to be slightly higher in the CS phase. Measurements at higher fields and lower temperatures are required to reveal to what extent Pauli limiting plays a role in determining $H_{c2}(0)$ in these materials.

The coherence length, ξ , can be calculated using the Ginzburg-Landau (GL) relation $\xi = (\Phi_0/2\pi H_{c2})^{1/2}$, where $\Phi_0 = 2.068 \times 10^{-15}$ Wb is the flux quantum²⁶. With $H_{c2}^{\text{NCS}}(0) = 125(1)$ kOe for NCS Re_3W , the estimated $\xi^{\text{NCS}}(0)$ is 5.13(2) nm. For CS Re_3W , the value of $\xi^{\text{CS}}(0)$ is deduced to be 4.73(5) nm from $H_{c2}^{\text{CS}}(0) = 147(3)$ kOe. Combining ξ and the standard expression $H_{c1} = \frac{\Phi_0}{4\pi\lambda^2} \left(\ln \frac{\lambda}{\xi} + 0.12 \right)$,²⁷ we estimate the magnetic penetration depth, $\lambda^{\text{NCS}}(0) = 257(1)$ nm and $\lambda^{\text{CS}}(0) = 141(11)$ nm for the NCS and CS phases of Re_3W , respectively. The value of $\lambda^{\text{NCS}}(0)$ is in good agreement with the value of 300(10) nm reported by Zuev *et al.*¹¹. We used the values of $\lambda(0)$ and $\xi(0)$ to calculate the GL pa-

TABLE III: Measured and derived superconducting and transport parameters of the non-centrosymmetric and centrosymmetric phases of Re_3W .

	NCS Re_3W	CS Re_3W
T_c^{onset} (K)	7.80 ± 0.05	9.40 ± 0.05
$H_{c1}(0)$ (Oe)	97 ± 1	279 ± 11
$H_{c2}(0)$ (kOe)	125 ± 1	147 ± 3
$\lambda(0)$ (nm)	257 ± 1	141 ± 11
$\xi(0)$ (nm)	5.13 ± 0.02	4.73 ± 0.05
$\kappa(0)$	50 ± 1	30 ± 3
$\rho(295 \text{ K})(\mu\Omega\text{m})$	1.7	2.1
l_{tr} (nm)	0.277	0.224

parameter $\kappa = \lambda/\xi$. They yield $\kappa^{\text{NCS}}(0) = 50(1)$ for the NCS phase and $\kappa^{\text{CS}} = 30(3)$ for the CS phase of Re_3W . The measured and derived superconducting and transport parameters of the NCS and the CS phases of Re_3W are listed in Table III.

IV. SUMMARY

In summary, we have shown that there are two different phases of Re_3W . One phase is non-centrosymmetric with an α -Mn structure and is superconducting with a T_c of 7.8 K. The other phase is centrosymmetric with a hexagonal structure and is also superconducting with a T_c of 9.4 K. Switching between the two phases is made possible by annealing (CS to NCS) or remelting (NCS to CS) the samples. The full hysteresis loops of the CS sample

of Re_3W show giant flux jumps, while no jumps are observed for the NCS sample. The temperature dependence of H_{c2} of the NCS phase for Re_3W can be fitted using the WHH model which yields $H_{c2}^{\text{NCS}}(0) = 125(1)$ kOe. In contrast, $H_{c2}(T)$ of the CS phase of Re_3W is linear at lower temperature and has a positive curvature nearer to T_c . A fit to the data gives $H_{c2}^{\text{CS}}(0) = 147(3)$ kOe. Using GL relations, the penetration depths are estimated to be $\lambda^{\text{NCS}} = 257(1)$ nm and $\lambda^{\text{CS}} = 141(11)$ nm and the coherence lengths are calculated to be $\xi^{\text{NCS}} = 5.13(1)$ nm and $\xi^{\text{CS}} = 4.73(1)$ nm at $T = 0$ K. Our results compare well with unpublished work¹² on the NCS phase of Re_3W . To the best of our knowledge, Re_3W is the first system of its kind to be found to exist as either a centrosymmetric or a non-centrosymmetric superconducting material. This, and similar systems if they exist, offer a good opportunity to study the interplay between the structure, spin-orbit coupling, and superconducting properties of intermetallic systems.

Acknowledgments

This work was supported by the Engineering and Physical Sciences Research Council (EPSRC) and the Science and Technology Facilities Council (STFC). Xpress Access neutron beam time on GEM was provided by the UK Science and Technology Facilities Council (STFC). PKB would like to thank the Midlands Physics Alliance Graduate School (MPAGS) for a studentship. The Quantum Design MPMS magnetometer and PPMS used in this research were obtained through the Science City Advanced Materials project: Creating and Characterizing Next Generation Advanced Materials project, with support from Advantage West Midlands (AWM) and part funded by the European Regional Development Fund (ERDF).

* P.K.Biswas@warwick.ac.uk

¹ E. Bauer, G. Hilscher, H. Michor, C. Paul, E. W. Scheidt, A. Griбанov, Y. Seropegin, H. Noël, M. Sigrist, and P. Rogl, Phys. Rev. Lett. **92**, 027003 (2004).

² L. P. Gor'kov and E. I. Rashba, Phys. Rev. Lett. **87**, 037004 (2001).

³ P. A. Frigeri, D. F. Agterberg, A. Koga, and M. Sigrist, Phys. Rev. Lett. **92**, 097001 (2004).

⁴ V. P. Mineev, Phys. Rev. B **71**, 012509 (2005).

⁵ N. Kimura, K. Ito, K. Saitoh, Y. Umeda, H. Aoki, and T. Terashima, Phys. Rev. Lett. **95**, 247004 (2005).

⁶ I. Sugitani, Y. Okuda, H. Shishido, T. Yamada, A. Thamizhavel, E. Yamamoto, T. D. Matsuda, Y. Haga, T. Takeuchi, R. Settai, et al., Journal of the Physical Society of Japan **75**, 043703 (2006).

⁷ N. Metoki, K. Kaneko, T. D. Matsuda, A. Galatanu, T. Takeuchi, S. Hashimoto, T. Ueda, R. Settai, Y. O-nuki, and N. Bernhoeft, J. Phys.: Condens. Matter **16**, L207 (2004).

⁸ T. Akazawa, H. Hidaka, H. Kotegawa, T. C. Kobayashi,

T. Fujiwara, E. Yamamoto, Y. Haga, R. Settai, and Y. Ōnuki, Journal of the Physical Society of Japan **73**, 3129 (2004).

⁹ J. K. Hulm and R. D. Blaugher, J. Phys. Chem. Solids **19**, 134 (1961).

¹⁰ R. D. Blaugher, A. Taylor, and J. K. Hulm, IBM J. Res. Dev. **6**, 116 (1962).

¹¹ Y. L. Zuev, V. A. Kuznetsova, R. Prozorov, M. D. Van- nette, M. V. Lobanov, D. K. Christen, and J. R. Thompson, Phys. Rev. B **76**, 132508 (2007).

¹² V. A. Kuznetsova, Ph.D. thesis, University of Tennessee (2007).

¹³ Y. Huang, J. Yan, Y. Wang, L. Shan, Q. Luo, W. Wang, and H.-H. Wen, Supercond. Sci. Technol. **21**, 075011 (2008).

¹⁴ P. Day, J. E. Enderby, W. G. Williams, L. C. Chapon, A. Hannon, P. G. Radaelli, and A. K. Soper, Neutron News **15**, 19 (2004).

¹⁵ B. H. Toby, Journal of Applied Crystallography **34**, 210 (2001).

- ¹⁶ A. C. Larson and R. B. Von Dreele, Los Alamos National Laboratory Report LAUR 86-748 (2000).
- ¹⁷ T. P. Orlando, E. J. McNiff, S. Foner, and M. R. Beasley, Phys. Rev. B **19**, 4545 (1979).
- ¹⁸ R. G. Mints and A. L. Rakhmanov, Rev. Mod. Phys. **53**, 551 (1981).
- ¹⁹ N. R. Werthamer, E. Helfand, and P. C. Hohenberg, Phys. Rev. **147**, 295 (1966).
- ²⁰ E. Helfand and N. R. Werthamer, Phys. Rev. **147**, 288 (1966).
- ²¹ S. V. Shulga, S.-L. Drechsler, G. Fuchs, K.-H. Müller, K. Winzer, M. Heinecke, and K. Krug, Phys. Rev. Lett. **80**, 1730 (1998).
- ²² I. Shigeta, T. Abiru, K. Abe, A. Nishida, and Y. Matsumoto, Physica C **392–396**, 359 (2003).
- ²³ Y. Takano, H. Takeya, H. Fujii, H. Kumakura, T. Hatano, K. Togano, H. Kito, and H. Ihara, Appl. Phys. Lett. **78**, 2914 (2001).
- ²⁴ A. B. Karki, Y. M. Xiong, N. Haldolaarachchige, S. Stadler, I. Vekhter, P. W. Adams, D. P. Young, W. A. Phelan, and J. Y. Chan, Phys. Rev. B **83**, 144525 (2011).
- ²⁵ R. Micnas, J. Ranninger, and S. Robaszkiewicz, Rev. Mod. Phys. **62**, 113 (1990).
- ²⁶ E. H. Brandt, Phys. Rev. B **37**, 2349 (1988).
- ²⁷ M. Tinkham, *Introduction to Superconductivity* (McGraw-Hill, New York, 1975).